Astron. Astrophys. 320, 109–114 (1997)

ASTRONOMY
AND
ASTROPHYSICS

The early-type binary KX Velorum⋆

Pavel Mayer[1], **Reinald Lorenz**[2], **and Horst Drechsel**[2]

[1] Astronomical Institute, Charles University, Švédská 8, 150 00 Praha 5, Czech Republic
[2] Dr. Remeis-Sternwarte Bamberg, Astronomisches Institut der Universität Erlangen-Nürnberg, Sternwartstraße 7, D-96049 Bamberg, Germany

Received 8 August 1996 / Accepted 10 September 1996

Abstract. A spectroscopic study of the double-lined OB-type binary system KX Vel is presented. Radial velocities were measured on 20 new CCD spectra and 4 high dispersion IUE SWP images. From a combination with early photographic data, the orbital period was found to be $26\overset{\mathrm{d}}{.}306$. The high precision radial velocity curve of the evolved primary component allowed for an accurate determination of the highly eccentric orbit (e = 0.59) using a SIMPLEX based fit procedure. The less luminous secondary main sequence component could be identified in spectra taken at phases shortly before and after the periastron passage, at which the high opposite radial velocities of both components made a deconvolution of the line blends possible. The combination of an earlier eclipse measurement with the new spectroscopic elements yields an ephemeris for expected future eclipse minima. Further spectroscopic observations (close to periastron phases) and photometric measurements (at eclipse epochs) are suggested to derive the absolute dimensions of the binary components of this detached close binary system.

Key words: binaries: spectroscopic – stars: early-type – stars: fundamental parameters – stars: KX Velorum

1. Introduction

Since the star HR 3527 (HD 75821; KX Velorum) has long been known for variable radial velocities. The variability was detected by Moore (1912; see also Campbell & Moore 1928) and confirmed by Buscombe (1962). Conti, Leep, and Lorre (1977) revealed the system being a double-lined binary, and Balona & Laing (1986) first observed part of an eclipse.

KX Vel is a bright early-type system (V = 5.1 mag at maximum). The spectral type is B0 III according to Morgan, Code, and Whitford (1955), while Conti et al. (1977) adopted O9.5 II. However, orbital elements and fundamental stellar parameters of this binary are still unknown. Therefore, the object was added to our list of early-type close binaries, for which spectroscopic and photometric observations have been collected during several observing seasons at ESO-La Silla, Chile, and Calar Alto Observatory, Spain (DSZA). The main aim of this program is to derive absolute dimensions and orbital elements for OB-type systems for a verification of modern stellar structure and close binary evolution theories. We report here on results of our spectroscopic analysis of KX Vel, which yielded the orbital period and a high-precision radial velocity curve of this binary.

2. Spectroscopy

Optical spectroscopic observations of KX Vel were made during several observing runs at the ESO-La Silla Observatory, Chile. In the years 1992 and 1993 we used the ESO 1.52m telescope with its ECHELEC spectrograph equipped with the RCA #13 CCD chip. The average linear dispersion was 3.8 Å mm^{-1}, and slit widths in the range $1\overset{''}{.}4$ to $2\overset{''}{.}5$ allowed for a resolving power of 23000 to 32000. The total spectral range was about 300 Åwide. Mostly for technical reasons (e.g., a cosmetic defect of the CCD detector coincided with the Hβ primary line in the first season), the spectral ranges covered were not always identical, but comprised in all cases Hβ and adjacent regions. In 1994 the star was observed with the ESO 1.4m CAT telescope feeding the ESO 3.6m Coudé Echelle Spectrometer CES. The short camera and the RCA #9 CCD chip were used. The linear dispersion was 2.6 Å mm^{-1}, and the slit width was $2\overset{''}{.}0$, equivalent to a resolving power of about 56000. Due to the high dispersion the useful spectral range was about 40 Å, and only one spectral line could be covered on the chip. The exposure times were mostly in the range 8 to 30 minutes, depending on atmospheric conditions. In two cases, cloudy weather required an extension to 45 minutes. The signal-to-noise ratios achieved were always within the range 150 to 200 (except for the spectrum taken at hel. JD $2449151\overset{\mathrm{d}}{.}501$, when it was only 60).

Our spectra were reduced using the ESO MIDAS image processing package. Especially, the wavelength calibration was carried out with great care. For each observing night, separate wavelength calibrations were performed, and then all Thorium-Argon comparison spectra taken in the same night were reduced in the manner of object spectra using the respectively achieved dispersion relation. In all cases the differences between the ta-

Send offprint requests to: P. Mayer

⋆ Based on observations collected at the European Southern Observatory, La Silla, Chile

Table 1. ECHELEC, CAT CES, and IUE SWP spectra

hel. JD 2 440 000+	Phase	Exp. (min)	Spectral range[a]
ECHELEC spectra			
8674.667	0.02	18	1
8675.595	0.05	20	1
8676.581	0.09	20	1
8677.638	0.13	20	1
8678.649	0.17	20	1
8760.494	0.28	20	2
8762.494	0.36	25	2
9025.538	0.36	30	3
9026.570	0.40	25	3
9028.544	0.47	25	3
9029.543	0.51	25	3
9146.515	0.96	45	4
9151.501	0.14	45	5
CAT CES spectra			
9448.512	0.44	15	He I 4922
9449.555	0.48	10	He I 4922
9450.554	0.51	12	He I 4922
9451.552	0.55	10	He I 4922
9452.527	0.59	8	Hα
9452.543	0.59	12	Hα
9454.556	0.66	12	He I 4922
IUE SWP spectra			
4042.399	0.93	2	SWP (6)
4389.666	0.13	3	SWP (6)
6251.226	0.89	2	SWP (6)
6532.518	0.59	2	SWP (6)

[a] Spectral ranges: 1: 4586-4908 Å; 2: 4642-4968 Å; 3: 4627-4954 Å; 4: 4823-5143 Å; 5: 4631-4957 Å; 6: 1250-1950 Å

Table 2. Radial velocities of KX Vel primary component

hel. JD 2 400 000+	Phase	$v_{\rm obs}$ (km s^{-1})	O-C (km s^{-1})	Wt.	Ref.[a]
19113.600	0.2899	-19.00	+3.43	0	1
19149.513	0.6551	+32.00	-4.79	0	1
19198.508	0.5176	+10.00	-1.52	0	1
37042.902	0.8508	+81.00	-13.93	0	2
37420.858	0.2183	-41.00	-9.24	0	2
37424.849	0.3701	-20.00	-8.92	0	2
42883.480	0.8734	+105.40	-0.08	2	3
44042.399	0.9283	+108.00	-27.31	0	4
44389.666	0.1292	-73.30	-34.99	0	4
46251.226	0.8942	+61.80	-54.59	0	4
46532.518	0.5872	-11.20	-34.75	0	4
48674.667	0.0184	+51.14	-0.51	4	5
48675.595	0.0537	-10.29	+0.89	4	5
48676.581	0.0912	-32.28	+1.28	4	5
48677.638	0.1313	-39.68	-1.34	4	5
48678.649	0.1698	-37.35	-0.60	4	5
48760.494	0.2810	-23.87	-0.22	5	5
48762.494	0.3570	-11.47	+1.49	5	5
49025.538	0.3563	-12.79	+0.27	5	5
49026.570	0.3956	-7.62	-0.27	5	5
49028.544	0.4706	+3.77	-0.23	5	5
49029.543	0.5086	+10.68	+0.63	5	5
49146.515	0.9551	+146.15	+0.25	5	5
49151.501	0.1447	-39.44	-1.25	5	5
49448.512	0.4352	-0.17	+1.27	3	5
49449.555	0.4748	+5.63	+0.97	3	5
49450.554	0.5128	+12.13	+1.39	3	5
49451.552	0.5507	+16.80	-0.29	3	5
49452.527	0.5878	+21.92	-1.73	3	5
49452.543	0.5884	+23.26	-0.50	3	5
49454.556	0.6649	+37.53	-1.36	4	5

[a] References: 1: Moore (1912); 2: Buscombe (1962); 3: Conti et al. (1977); 4: IUE data; 5: ESO ECHELEC and CAT data

ble values of the Th-Ar emission lines and the measured wavelengths were much smaller than 0.01 Å or about 1.3 km s^{-1}.

Due to the various spectral ranges used, the lines suitable for positional measurements also differ in spectra obtained in different seasons. A journal of our new spectra is found in Table 1, giving technical information about the individual exposures. As a typical example an ECHELEC CCD spectrum taken with the ESO 1.52m telescope on JD 2449028 at orbital phase 0.47 is shown in Fig. 1. The exposure time was 25 minutes, which corresponds to a phase resolution of better than 10^{-3}. The different orders have been normalized and merged to cover the wavelength range from about 4640 to 4940 Å. Identifications of some of the more prominent lines are given, and a few CCD artifacts are correspondingly marked. The radial velocities derived from the ESO ECHELEC and CAT spectra, complemented by data from other sources, are listed in Table 2; the O-C values given there refer to a fitted radial velocity curve, which is further discussed below.

In our complete sample of optical spectra we measured a total of 275 lines (of H, He I, He II, C III, N III, O II, Si III, and Si IV). The features were fitted by Gaussian profiles. The blends between primary and secondary line components were resolved using a multiple Gaussian fit procedure of the MIDAS package yielding radial velocities among other line parameters. It is obvious that some lines exhibit systematic shifts of the order of a few km s^{-1} compared with the mean velocities of most other lines, and others show a larger than average amount of intrinsic scattering. For instance, most Hβ primary lines were clearly systematically off the mean curve. Since a CCD defect was intersecting the Hβ profiles in some of our spectra, this line was not used for the calculation of primary velocities ; for unknown reasons, the O II 4906 and 4925 lines also deviated by about 20 km s^{-1} and were not evaluated for the construction of the mean radial velocity curve; other mostly weaker lines with relatively high positional uncertainties were discarded as well. Since a sufficiently large number of useful lines was available, only those with the smallest errors of their Gaussian fits and without systematic deviations from the overall mean velocity curve were considered for a determination of orbital elements. For this purpose we finally selected the lines Hα, He I 4713 and

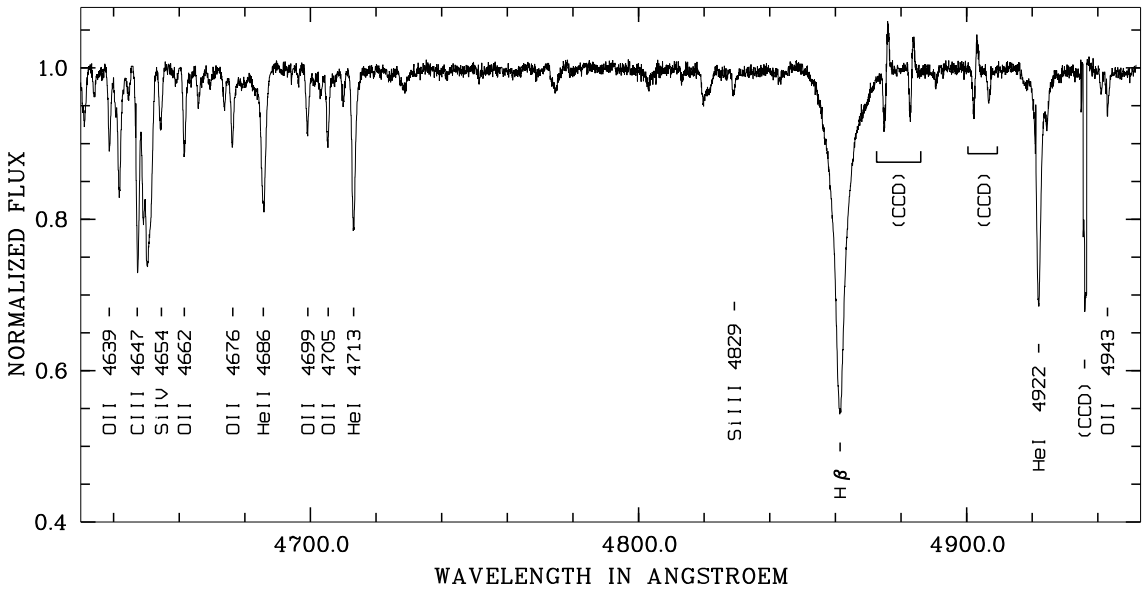

Fig. 1. Merged ESO 1.52m ECHELEC spectrum taken on JD 2449028 at orbital phase 0.47 (exposure time: 25 min)

4922, He II 4686, C III 4647 and 4666, O II 4674 and 4676, and Si IV 4654. Average velocities of the primary component were calculated as unweigthed means of the values of these individual lines, and are listed in Table 2 in the column labeled $v_{\rm obs}$.

The total time base of observations could be extended by complementing our new spectroscopic data by three earlier photographic measurements of Moore (1912), three others by Buscombe (1962), a value of Conti et al. (1977), and four high dispersion IUE images, which are also listed in Table 2. For the determination of orbital elements, the radial velocities were weighted according to their quality and origin with factors (see column headed *Wt.*), which vary from 2 up to 5. Weight 0 for the old photographic and IUE spectra means that these data were exclusively used for the period determination, but not for the final orbital solution. Weight factors of 3 to 5 were given to our high resolution electronic data, depending on signal-to-noise ratios and the number of lines used for the calculation of radial velocities.

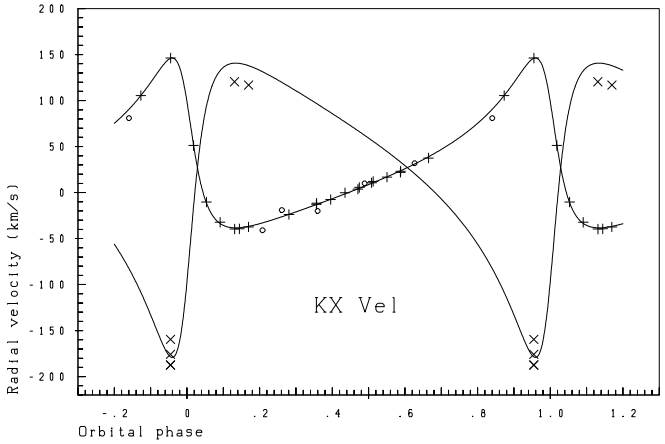

Fig. 2. Radial velocity curves of primary and secondary components according to elements of Table 3; primary velocities from CCD observations are shown as plus signs, photographic data as circles, and secondary velocities as crosses

3. Period and orbital elements

The degree of redundancy in the phase coverage of the radial velocities following from our different observing seasons first allowed for a rough determination of the hitherto unknown orbital period. A more refined value was then found by extending the time span covered by observations with the earlier published velocities, while the final exact value of P = 26$^{\rm d}$.30624 was adjusted in the course of the numerical orbital element solution.

We have also used four IUE high dispersion SWP spectra for the determination of the period. Radial velocities of about 30 photospheric lines in each spectrum were determined relative to interstellar lines. The average values for each spectrum together with their O-C values are contained in Table 2. However, in our optical spectra no interstellar lines could be evaluated. Only Buscombe & Kennedy (1962) published a value for Ca II of +20 km s^{-1}, which is based on a single plate. Therefore the correction to be added to the IUE velocities is known with only low accuracy. A larger value of the correction is suggested by the comparison with the best fitting radial velocity curve: with the orbital parameters of Table 3, the correction then amounts to +37.9 km s^{-1}. Due to this uncertainty, the radial velocities derived from the high resolution IUE spectra were therefore only used for a preliminary period determination, but not for the final orbital solution.

The optimization of the orbital elements e (eccentricity), ω (periastron length), K_1 (velocity amplitude), γ_0 (systemic veloc-

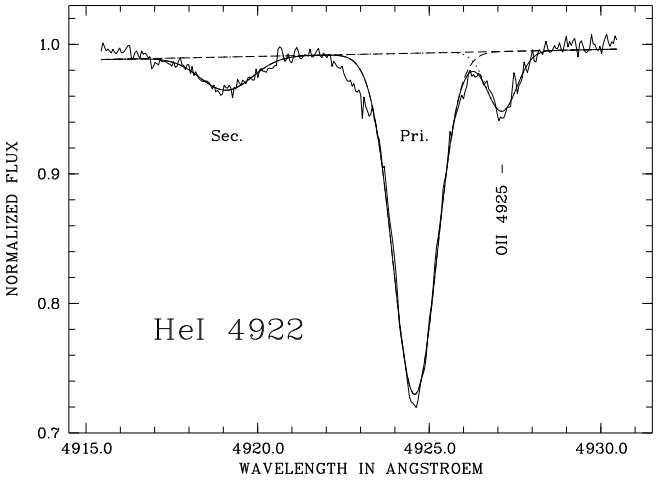

Fig. 3. He I 4922 line profile at phase 0.955 (on JD 2449146); the Gaussian fit of the primary and well separated secondary components is shown as solid line; another, weaker primary line (O II 4925) is shown as well

Table 3. Orbital elements of KX Vel

Period	$26\overset{d}{.}30624 \pm 0\overset{d}{.}00110$
semi-amplitude K_1	92.30 ± 0.3 km s^{-1}
systemic velocity	27.17 ± 0.2 km s^{-1}
eccentricity	0.591 ± 0.006
length of periastron	$60\overset{\circ}{.}62 \pm 0\overset{\circ}{.}21$
time of periastron	hel. JD $2419105\overset{d}{.}97 \pm 0\overset{d}{.}15$

ity), P (orbital period), and T_0 (time of periastron passage) was achieved using a code written by Raja (1996), which is based on the SIMPLEX algorithm. The resulting elements are found in Table 3. The corresponding best fitting radial velocity curve is plotted in Fig. 2 together with the observations. O-C values for all lines measured in the ESO spectra relative to the theoretical curve are given in Table 4. From these data, any systematic deviations and the amount of intrinsic scattering for individual lines are immediately apparent; hence this information can be used for checking the behavior and usefulness of different lines. It should be noted that the achieved fit quality is very good, yielding a small standard deviation of 0.93 km s^{-1} for the sample of lines with weights 3 to 5, and of about 2 km s^{-1} for the complete sample including the photographic data and the value of Conti et al. (1977). Therefore the accuracy of the orbital parameters is remarkably high.

Though the formal errors of the fitted parameters are very small, the real values of the orbital elements might still be somewhat different, because the phase interval from 0.7 to 1.0 is only scarcely covered by our data. Nevertheless, the star might qualify as a prime object among those providing precise data on masses and radii (see Sect. 4).

Clearly, the orbit is strongly eccentric. As can be seen from the radial velocity curve (Fig. 2), there are only two relatively narrow phase intervals around phases $0.92 - 0.98$ and $0.1 - 0.2$ shortly before and after the periastron phase, respectively, during which the separation of primary and secondary lines can be expected sufficiently large to allow for a deconvolution of their line profiles. By chance, Conti et al. (1977) took their spectrum near the time of periastron (at phase 0.87), so that they were able to identify some lines of the secondary star for the first time. At most other phases, the secondary features are severely blended with the primary lines. Due to the large luminosity ratio between primary and secondary, the lines of the companion are otherwise hardly distinguishable. One of our spectra was fortunately taken at the most convenient phase 0.96, where the secondary lines are found at maximum blue-shifted position and show nearly no overlap with the broad primary features. The presence of secondary features could be confirmed for Hβ, He I 4922 (see Fig. 3), He I 5016, and He I 5048. Unfortunately it is much more difficult to discern the secondary lines at opposite phases, when they appear on the red side of the primary lines. There is a disturbing line (O II 4925) close to He I 4922, which prevents a clear identification of the red-shifted secondary component. Most other lines covered by our specta are too weak (or affected by blends) to be attributed to the secondary component unambiguously. The only spectral features, for which a marginal detection of the secondary star was possible in our spectra taken at phases 0.13 and 0.17, were He I 4713 and He II 4686. The measurement of the secondary line positions in these spectra is rather uncertain, however, due to the weakness of these features. The measured velocities are listed in Table 5. Possibly, other lines (e.g. He I 5876) outside the spectral range covered by our spectra would reveal the secondary component more clearly at these phases.

Therefore, at present K_2 is less accurately known than K_1, since the secondary lines were measured at three epochs only. From the Hβ, He I 4922, 5016, and 5048 secondary lines at phase 0.96 and the He I 4713 lines at phases 0.13 and 0.17, a best fitting K_2 value of 159.9 km s^{-1} is found, if the other orbital elements are kept fixed at the values derived from the primary curve. The mass ratio then amounts to 0.58 ± 0.03, and the projected semi-axes come out as $a_1 \sin i = 38.7$ R$_\odot$ and $a_2 \sin i = 67.0$ R$_\odot$; for the masses we find lower limits of $M_1 \sin^3 i = 14.5$ M$_\odot$, and $M_2 \sin^3 i = 8.4$ M$_\odot$.

4. Discussion

The time of minimum observed by Balona & Laing (1986) – JD $2446438\overset{d}{.}60$ – corresponds to orbital phase 0.0168 (if the periastron time is used as zero epoch), and agrees very well with the expected epoch of secondary minimum resulting from the elements given in Table 3 (phase 0.0175). Hence the difference between the observed and calculated minimum epochs is not larger than the estimated observational error. The orbital solution suggests that the primary minimum should occur at phase 0.7286. However, since the separation of the stellar components is larger during a possible eclipse of the primary component than during secondary minimum, a primary minimum may not necessarily exist at all. Yet should it be observable, it would be rather shallow, presumably with a depth of only several hundredths of magnitude. The observations of Balona & Laing (1986) cover

Table 4. Lines of KX Vel primary component measured in ESO spectra (O-C in km s^{-1} relative to best fitting curve for elements of Table 3)

hel. JD 2 440 000+	O II 4591	O II 4596	Si IV 4631	N III 4634	O II 4639	N III 4641	O II 4642	C III [a] 4647	O II 4649	C III 4650	C III 4651
8674.667	-5.55	-1.36	-18.88	-11.14	-9.88	-6.02	-6.03	-2.21	-13.19	-6.11	-8.06
8675.595	1.66	4.61	-17.02	-6.65	-1.46	-6.62	-3.39	0.50	-2.07	-2.07	-13.66
8676.581	5.58	5.28	-15.53	-6.44	-2.52	1.37	-0.56	2.06	0.14	-3.72	-19.82
8677.638	0.12	-0.16	-16.37	-5.98	-5.29	-2.69	-3.33	-1.98	-7.77	-5.83	-15.47
8678.649	3.47	1.88	-11.76	-9.79	-3.93	-2.62	-2.61	-1.27	-2.55	-3.83	
8760.494								-1.80	-12.11	14.97	0.79
8762.494								-0.32	-3.90	-2.90	-15.14
9025.538			-11.76	-7.86	-4.60	-4.60	-3.94	-1.34	-5.20	-5.84	-18.72
9026.570			-13.88	-7.60	-4.79	-8.01	-4.78	-2.18	-4.11	-6.68	-22.79
9028.544			-14.70	-8.22	-6.27	-8.20	-4.33	-1.74	-7.54	-5.61	-13.98
9029.543			-17.11	-4.17	-3.52	-8.04	-2.23	-0.94	-3.53	-4.82	-18.99
9146.515											
9151.501					-3.42	-4.06	-4.70	-0.79	-4.65	-7.22	-27.20

	Si IV [a] 4654	O II 4662	C III [a] 4666	O II [a] 4674	O II [a] 4676	He II [a] 4686	O II 4699	O II 4705	O II 4710	He I [a] 4713	Si III 4829
8674.667	2.87	-5.58	-1.12	2.65	-0.59	-0.81	-11.67	-7.26	-7.94	-4.34	
8675.595	1.81	-2.67	3.12	-0.07	-0.06	0.48	-11.48	-4.44	-6.33	0.48	
8676.581	-0.47	0.88	2.83	-0.96	-0.30	4.76	-7.78	-3.27	-3.87	1.06	
8677.638	0.01	-4.43	-1.18	-3.67	-1.09	0.14	-10.46	-4.66	-6.53	-1.60	
8678.649	-0.57	-1.79	0.44	-2.34	-1.68	0.84	-7.23	-3.98	-3.31	0.35	
8760.494	1.44	-4.34	2.10	-1.09	-3.01	1.36	-8.69	-5.48	-9.29	-0.56	
8762.494	5.48	-2.25	3.53	0.31	-1.52	2.74		-2.25	-0.97	2.02	
9025.538	1.27	-5.13	4.52	-1.87		0.62	-6.85	-5.55	-4.89	0.66	
9026.570	1.71	-4.70	2.38	-1.45	-2.73	0.38	-9.03	-3.91	-7.71	0.38	
9028.544	2.13	-4.30	0.84	-0.44	-3.01	-0.57	-7.54	-5.53	-4.89	1.29	
9029.543	2.27	-2.89	2.25	0.95	-0.97		-5.46	-2.91	-5.46	1.98	
9146.515											0.19
9151.501	-3.33	-6.51	-0.05	-1.30	0.64		-4.35	-1.76	-6.83	-0.64	

	Hβ 4861	O II 4906	He I [a] 4922	O II 4925	O II 4941	O II 4943	N II 5001	N II 5005	He I 5016	He I 5048	Hα [a] 6576
8674.667	-1.85										
8675.595	15.23										
8676.581	9.06										
8677.638	15.25										
8678.649	15.23										
8760.494	6.70	19.58	-0.51	-13.35							
8762.494	10.11	17.33	-0.33	-19.26							
9025.538	4.48		-1.99	-17.87							
9026.570	4.03	13.88	-0.68	-17.77							
9028.544	3.31	14.89	-0.32	-22.29							
9029.543		15.93	-1.14	-16.42							
9146.515	4.05	19.65	0.87	-7.80	-5.28	-5.95	2.44	2.32	-0.12	-0.01	
9151.501	10.15		-3.25	1.80							
9448.512			1.27	-19.50							
9449.555			0.97	-18.58							
9450.554			1.39	-17.55							
9451.552			-0.29	-12.56							
9452.527											-1.73
9452.543											-0.50
9454.556			-1.36	-8.75							

[a] lines used for radial velocity curve of KX Vel primary component

Table 5. Radial velocities of KX Vel secondary component

hel. JD 2 440 000+	Phase	Line	v_{obs} (km s^{-1})
9146.5145	0.955	Hβ	-159.62
	0.955	He I 4922	-187.62
	0.955	He I 5016	-175.78
	0.955	He I 5048	-187.29
8677.6383	0.131	He I 4713	+120.35
	0.131	He II 4686	+62.25:
8678.6494	0.170	He I 4713	+116.89
	0.170	He II 4686	+70.93:

Table 6. Equivalent widths (in Å) of lines in the spectrum taken at phase 0.955 on JD 2449146

Line	Primary	Secondary
Hβ	1.611	0.363
He I 4922	0.424	0.050
He I 5016	0.276	0.036
He I 5048	0.120	0.010

only the descending part of a secondary minimum, the total duration of which can be extrapolated to be about $0^d.50$. Hence the primary minimum might then last for about $1^d.56$.

Combining Balona & Laing's (1986) minimum time with our newly found period, the following ephemeris for eclipse minima can be given as:

Pri. min.: hel. JD $2446457^d.32 + 26^d.30624 \cdot E$
Sec. min.: hel. JD $2446438^d.60 + 26^d.30624 \cdot E$.

Due to an expected, but so far unconfirmed rotation of the line of apsides, the last digit of the period value might be different in the expressions for primary and secondary minima.

In our spectrum taken at phase 0.955, in which the secondary line components can be readily resolved at least in the Hβ feature and for the He I 4922, 5016, and 5048 transitions, equivalent widths of the primary and secondary components were measured and are listed in Table 6. It should be noted that these equivalent widths refer to the composite continuum of both binary components. Therefore the values may be used for an estimate of the luminosity ratio of the two stars (if equal abundances are assumed), but have no meaning if compared to equivalent widths of single stars of similar type. Since, however, abundance anomalies are rather common for interacting binary components in an evolutionary stage after large-scale mass transfer, any conclusions drawn from line strengths must thoroughly account for such evolutionary effects. In turn, these data might be helpful for the determination of the evolutionary state, if sufficiently accurate absolute dimensions are at hand for a comparison with evolutionary calculations.

In the case of KX Vel, the ratio of He I line strengths (in the sense primary relative to secondary) is considerably larger than the ratio of Hβ lines, which more likely corresponds to the true luminosity ratio of the binary components. According to theory (see, e.g., Popper 1993) one should expect the He I line widths to be smaller for stars with lower log g values, which is merely compatible with the fact that the lines of the evolved primary are so much stronger than those of the unevolved secondary star, which has the higher log g. Also the Balmer line widths depend on log g, so that their line strength ratio should not be considered as a direct measure for the stellar luminosities either, at least without any further more refined investigation.

The relatively strong helium lines of the primary may be partly explained by the fact that the atmospheres of evolved early-type stars are enhanced by helium (see, e.g., Gies & Lambert 1992). KX Vel is a well detached system, even at periastron phase, and certainly the more luminous primary (with its luminosity class of II-III) is the farther evolved component, while the secondary is still on the main sequence. The contrary was, e.g., observed in the previously studied case of the semi-detached massive binary AB Cru (Lorenz et al. 1994): the Roche lobe filling secondary star of this system showed strong helium enhancement, because it was stripped off its outer hydrogen layers due to large-scale mass loss during the rapid mass transfer phase. Any such strong interaction effects can, however, be excluded for the KX Vel system in the present state as well as for the past evolutionary history.

Yet several aspects render KX Vel as an important system to be closely followed up in the future: it belongs to the small group of early-type systems, for which a determination of accurate stellar parameters is needed for a comparison with modern theories of interior structure and stellar evolution. It has been demonstrated that high quality radial velocity curves can be established, and correspondingly precise elements and stellar parameters can be derived. It will be essential to obtain further spectra at orbital phases poorly covered so far; especially spectra at the short epochs of high radial velocities, which are suitable for a deconvolution of the secondary lines, will be important to pin down the mass ratio more accurately. For this purpose, it is also suggested to collect photometric data during suspected eclipse periods.

Acknowledgements. This work was supported by the *Deutsche Forschungsgemeinschaft, DFG* grants Dr 131/8-2,3 and 436 CSR 113/39/1. We appreciate the assistance of the staff of the *ESO-La Silla* observatory and of the *ESA VILSPA IUE* ground station.

References

Balona, L.A., Laing, J.D. 1986, MNRAS 223, 621
Buscombe, W. 1962, MNRAS 124, 189
Buscombe, W., Kennedy, P.M. 1962, MNRAS 124, 195
Campbell, W.W., Moore, J.H. 1928, Lick Obs. Publ. 16
Conti, P.S., Leep, E.M., Lorre, J.J. 1977, ApJ 214, 759
Gies, D.R., Lambert, D.L. 1992, ApJ 387, 673
Lorenz, R., Mayer, P., Drechsel, H. 1994, A&A 291, 185
Moore, J.H. 1912, Lick Obs. Bull. 7,96
Morgan, W.W., Code, A.D, Whitford, A.E. 1955, ApJS 2, 41
Popper, D.M. 1993, PASP 105, 721
Raja, T. 1996, Thesis, Charles University, Praha

This article was processed by the author using Springer-Verlag LaTeX A&A style file *L-AA* version 3.